

Non-Hermitian Aharonov-Bohm Cage in Bosonic Bogoliubov-de Gennes Systems

Kunling Zhou,¹ Bowen Zeng,^{2,*} and Yong Hu^{1,†}

¹*School of Physics, Huazhong University of Science and Technology, Wuhan 430074, P. R. China*

²*Hunan Provincial Key Laboratory of Flexible Electronic Materials Genome Engineering, School of Physics and Electronic Sciences, Changsha University of Science and Technology, Changsha 410114, P. R. China*

The non-Hermitian Aharonov-Bohm (AB) cage is a unique localization phenomenon that confines all possible excitations. This confinement leads to fully flat spectra in momentum space, which are typically accompanied with the degeneracy with various types. Classifying the degeneracy type is crucial for studying the dynamical properties of the non-Hermitian AB cage, but the methods for such classification and their physical connections remain not very clear. Here, we construct a non-Hermitian AB cage in a bosonic Bogoliubov-de Gennes (BdG) system with various types of degenerate flat bands (DFBs). Using the transfer matrix, we demonstrate the localization mechanism for the formation of AB cage and derive the minimal polynomial in mathematics for classifying the degeneracy types of DFBs, thus providing comprehensive understanding of the correspondence among the degeneracy type of DFBs, the minimal polynomial, and the transfer matrix. With such correspondence, we propose a scheme to realize highly degenerate flat bands.

I. INTRODUCTION

Flat bands refer to dispersion relations that are independent of momentum, leading to zero group velocity and the consequent localization of excitations [1–16]. The Aharonov-Bohm (AB) cage [17–20] is a unique localization phenomenon that confines all possible excitations, thereby giving rise to entirely flat spectra across all bands. This character renders the AB cage a good platform for exploring the strongly correlated physics. The formation of AB cage arises from the complete destructive interference induced by the interplay between an external gauge field and the lattice geometry [18, 21, 22]. A recent study [23] introduced a novel non-Abelian AB cage, in which the condition for the destructive interference is generalized to the nilpotent interference matrix. This generalization enables different AB cages to be characterized by different nilpotent indices that are governed by the order of exceptional points (EPs), a unique spectral degeneracy phenomenon with the collapse of the eigenstates space [24, 25] in the non-Hermitian systems. Thus, the formation of an AB cage generally leads to the flat bands with degeneracy, which are referred to as degenerate flat bands (DFBs) in this work.

The degeneracy in DFBs endows the AB cage with abundant physics such as enhanced sensitivity to perturbation arising from the nonlinear spectral structure in the vicinity of the EPs [26–30]. Recently, the energy degeneracy associated with high-order EPs has attracted much attention [31–34] and there is a growing demand for DFBs with higher degeneracy degrees [35–39]. One of the driving factors behind this is that additional filling selections of highly degenerate flat bands pave the way for a broader range of strongly correlated physics phenomena [39]. DFBs with higher degeneracy degrees usually exhibit various types of degeneracy, which can manifest as the diabolical points (DPs) type, the EPs type or a combination of them [40–44]. Classifying these

degeneracy types holds great significance. For example, for DFBs with different types, the excitations transition in different ways, causing the AB cage to exhibit distinct dynamical properties and local structures [23, 45]. A mathematical approach to classify the degeneracy type of DFBs involves utilizing the minimal polynomial of the matrix [46], but which lacks physical intuition. It is hypothesized that the potential physical connections might be embedded within the transfer matrix [47, 48], which represents the transition probability between two states. However, such connections have yet to be fully understood.

To comprehensively illustrate the relationship among the degeneracy type of DFBs in the AB cage, the minimal polynomial, and the transfer matrix, we choose the bosonic Bogoliubov-de Gennes (BdG) system as a specific example. One reason is that the non-Hermitian nature of dynamical matrices of BdG systems renders them more convenient to realize a non-Hermitian AB cage experimentally without involving gain and loss [49–52]. The other reason is that the inherent particle-hole symmetry and pseudo-symmetry [53] in BdG systems enable the realization of DFBs with high degeneracy degrees.

In such a non-Hermitian AB cage constructed in bosonic BdG system, by tuning the system parameters, we demonstrate a flexible control over the degeneracy type of flat bands, ranging from DPs type to higher-order EPs type. Unlike the conventional method of distinguishing degeneracy types based on the response to external perturbations, here we establish the correspondence between parameter-dependent transfer matrix and the minimal polynomial that can be used to determine the degeneracy types of DFBs. Meanwhile, we also uncover the localized mechanism for the formation of AB cage by investigating the limitation of the transfer matrix on the prohibited propagation paths. Applying such correspondence to the system with N coupled chains, the transfer matrix can be designed to achieve DFBs with

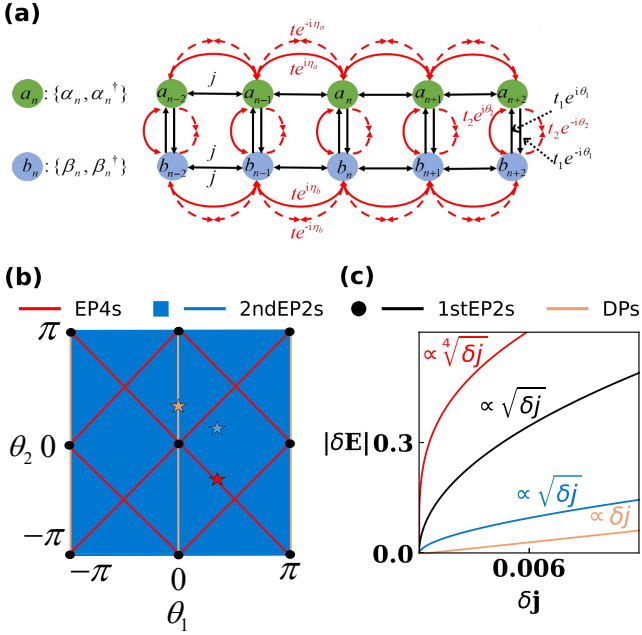


FIG. 1. (a) Schematic diagram of the ladder model, consisting of coupled two Kitaev-Majorana chains, where each site includes both particle and hole degrees of freedom. The conjugated coupling and two-boson creation/annihilation processes are denoted by the black lines, red solid/dashed lines, respectively. (b) The θ_1 - θ_2 phase diagram of degeneracy type of DFBs, where the red lines, yellow lines, blue regions and black dots correspond to EP4s type, DPs type, 1stEP2s type and 2ndEP2s type in the energy band. (c) The dependence of the absolute value of eigenvalues variation on the perturbation δj for different types of DFBs, when $j = t = 2$ and the wave vector is chosen as $k = 0$. The parameter choices are $\{t_1 = t_2 = 2, \theta_1 = -\theta_2 = \pi/3\}$ for the EP4s type, $\{t_1 = 2\sqrt{3}, t_2 = 2, \theta_1 = \pi/3, \theta_2 = \pi/6\}$ for the 2ndEP2s type, $\{t_1 = t_2 = 2, \theta_1 = \theta_2 = 0\}$ for the 1stEP2s type, and $\{t_1 = 1, t_2 = 2, \theta_1 = 0, \theta_2 = \pi/3\}$ for the DPs type. The θ_1, θ_2 for the 1stEP2s type are located at the origin point, while those for the other types are marked with pentagrams in their corresponding colors in (b).

$2N$ -order EPs type degeneracy.

II. MODEL

We consider a ladder model consisting of two identical bosonic Kitaev-Majorana chains, denoted as chain “a” and chain “b”, as shown in Fig. 1(a). The conjugated coupling (black lines) and number non-conservation coupling including two-boson creation and annihilation processes (red solid and dashed lines) are parameterized by j and $t e^{\pm i\eta_{(a,b)}}$ for chains (“a”, “b”). Their counterparts for the rungs of the ladder are parameterized by $t_1 e^{\pm i\theta_1}$ and $t_2 e^{\pm i\theta_2}$, respectively. The Hamiltonian for this system is

given by

$$H = \sum_n j \alpha_n^\dagger \alpha_{n+1} + j \beta_n^\dagger \beta_{n+1} + t_1 e^{i\theta_1} \alpha_n^\dagger \beta_n + t_2 e^{i\theta_2} \alpha_n^\dagger \beta_n^\dagger + t e^{i\eta_a} \alpha_n^\dagger \alpha_{n+1}^\dagger + t e^{i\eta_b} \beta_n^\dagger \beta_{n+1}^\dagger + h.c., \quad (1)$$

where $(\{\alpha_n, \alpha_n^\dagger\}, \{\beta_n, \beta_n^\dagger\})$ denote the creation and annihilation operators for chains (“a”, “b”) on n -site. Without loss of generality, we choose t_1, t_2, t , and j as real numbers, while η_a, η_b, θ_1 , and θ_2 are phase factors related to the gauge choice. Considering the gauge invariance for non-Abelian gauge field [54, 55], two gauge degrees of freedom remain, as detailed in the Appendix A. Consequently, we can always choose a gauge where $\eta_a = 0$ and $\eta_b = 0$, while keeping phase factors θ_1 and θ_2 . In this gauge, the Hamiltonian in momentum space is expressed as

$$H(k) = \sum_k 2j \cos k \alpha_k^\dagger \alpha_k + 2j \cos k \beta_k^\dagger \beta_k + (t_1 e^{i\theta_1} \alpha_k^\dagger \beta_k + t_2 e^{i\theta_2} \alpha_k^\dagger \beta_{-k}^\dagger + t \cos k \alpha_k^\dagger \alpha_{-k}^\dagger + t \cos k \beta_k^\dagger \beta_{-k}^\dagger + h.c.). \quad (2)$$

In the bosonic BdG systems, the evolution of mode $\psi(k) = [\alpha_k, \beta_k, \alpha_{-k}^\dagger, \beta_{-k}^\dagger]^\top$ is governed by the Heisenberg equation of motion,

$$i \frac{d\psi(k)}{dt} = \tilde{H}(k) \psi(k). \quad (3)$$

Here, $\tilde{H}(k)$ is the dynamical matrix associated with Eq. (2). A conventional approach for solving the eigenvalues of $\tilde{H}(k)$ is to express $\tilde{H}(k)$ in terms of Dirac gamma matrix in Dirac representation [56],

$$\tilde{H}(k) = 2j \cos k \gamma^0 + t_1 \cos \theta_1 \gamma^1 \gamma^5 + it_1 \sin \theta_1 \gamma^1 \gamma^3 + 2t \cos k \gamma^0 \gamma^5 + t_2 \cos \theta_2 \gamma^1 + it_2 \sin \theta_2 \gamma^0 \gamma^1. \quad (4)$$

Here $\gamma^i = i\sigma_2 \otimes \sigma_i$ for $i = 1, 2, 3$, $\gamma^0 = \sigma_3 \otimes I_2$ and $\gamma^5 = \sigma_1 \otimes I_2$ with σ_i being the Pauli matrix. Utilizing the properties of γ matrix and squaring two sides of the equation twice yield the annihilating polynomial [46] of $\tilde{H}(k)$ as

$$(\tilde{H}(k)^2 - (\lambda - \sqrt{\delta})I_4)(\tilde{H}(k)^2 - (\lambda + \sqrt{\delta})I_4) = 0 \quad (5)$$

with parameters $\lambda^2 = t_1^2 - t_2^2 + 4(j^2 - t^2) \cos^2 k$ and $\delta = 4 \cos^2 k ((j t_1 \cos \theta_1 - t t_2 \cos \theta_2)^2 + (j^2 - t^2) t_1^2 \sin^2 \theta_1)$. According to the Hamilton-Cayley theorem [46, 57, 58], the annihilating polynomial Eq. (5) is identical to the character polynomial and the roots $\pm \sqrt{\lambda \pm 2\sqrt{\delta}}$ serve as the eigenvalues of $\tilde{H}(k)$. It is clear that when $t = j$ and $t_1 \cos \theta_1 = t_2 \cos \theta_2$, the dispersion relation of $\tilde{H}(k)$ is simplified to $\pm \sqrt{t_1^2 - t_2^2}$ independent of momentum, exhibiting a non-Hermitian AB cage with completely flat bands.

Such flat bands are degenerated involving at least two degeneracy degrees. Under the constraint $t_1 \cos \theta_1 = t_2 \cos \theta_2$, Fig. 1(b) shows the θ_1 - θ_2 phase diagram for DFBs. Our system allows four types of degeneracy, including a DPs type, two kinds of EP2s types, and a fourth-order EPs (EP4s) type, as shown in Fig. 1(b). While previous studies focused on DFBs associated with single type of degeneracy such as EP2s [42–44], EP3s [41], and EP4s [43], our work unifies these types within a single system and reveals the correspondence between the degeneracy types and the transition properties of the AB cage, as discussed in Section. IV. The system exhibits DPs type DFBs when $\theta_1 = n_1\pi$, $\theta_2 \neq n_2\pi$ and $n_1, n_2 \in \mathbb{Z}$ with $E = \pm\sqrt{t_1^2 - t_2^2}$, as verified by the linear dependence of the absolute value of eigenvalues on perturbation δj [see Fig. 1(c)]. The realization of EP4s requires $\theta_1 \neq n_1\pi$ and $\theta_1 \pm \theta_2 = n_2\pi$ with $E = 0$. In this case, under perturbation δj , the eigenvalues variation $\delta|E| \propto \sqrt[4]{\delta j}$, as shown in Fig. 1(c). There are two kinds of EP2s in Fig. 1(b), where the first EP2s (1stEP2s) type emerges at the intersection of EP4s lines and DPs lines and the second EP2s (2ndEP2s) lies within blue regions. The absolute value of eigenvalues for both two EP2s types exhibit $\sqrt{\delta j}$ with different constant factors. For each type of DFBs, the minimum polynomial and excitation transition varies, as will be discussed later.

III. THE LOCALIZATION MECHANISM OF THE NON-ABELIAN AB CAGE

To provide insights behind rich degeneracy types of DFBs in our system and uncover the localization mechanism of the non-Abelian AB cage in real space, we consider an excitation in the ladder model and trace its transition using the transfer matrix, as shown in Fig. 2.

We firstly elucidate the method of transfer matrix used here. In our system, the particle and hole degrees of freedom on a single site can be expressed as a two-component operator $\gamma_{a_n(b_n)} = [\alpha_n(\beta_n), \alpha_n^\dagger(\beta_n^\dagger)]^\top$. The Heisenberg equation of motion for the operator γ_{a_n} is thus given by

$$i\dot{\gamma}_{a_n} = \sum_m (U_{a_n, a_m} \gamma_{a_m} + U_{a_n, b_m} \gamma_{b_m}). \quad (6)$$

Here, both of U_{a_n, a_m} and U_{a_n, b_m} are the 2×2 transfer matrices that characterize the transition probability from site a_m and b_m to site a_n . A similar analysis applies to γ_{b_n} . Now, the conjugate coupling and number non-conserving coupling between two sites in Fig. 1(a) can be replaced by these transfer matrices, which are similar to the translational-invariant link variables produced by a non-Abelian gauge field [23, 55]. From this perspective, these transfer matrices typically do not commute with each other. Due to the translation symmetry of system, we can use four types of transfer matrices U_r , U_l , U_\uparrow and U_\downarrow to represent various transitions between different

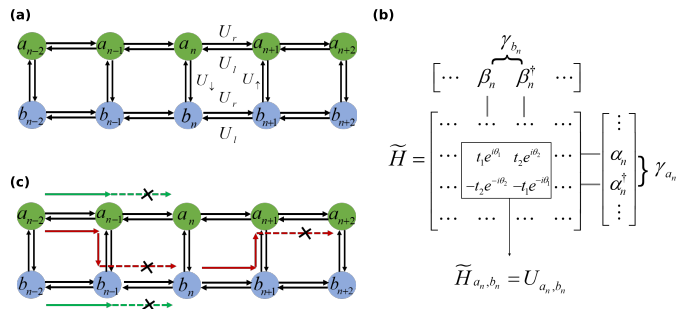


FIG. 2. (a) The transfer matrix U between different sites, where U_l (U_r , U_\uparrow , U_\downarrow) denotes the leftward (rightward, upward, downward) transition. (b) The dynamical matrix \tilde{H} in real space involving all possibilities of propagation, which is exemplified by a specific transfer matrix U_{a_n, b_n} from b_n to a_n . (c) Schematic diagram of the localization mechanism for the formation of DFBs, which can be simplified as the excitation at the n -th column cannot hop to the $(n \pm 2)$ -th column along the red and green propagation paths.

sites, as depicted in Fig. 2(a) and these transitions are thus non-Abelian. Here, U_r and U_l have the form of

$$U_r = U_{a(b)_{n+1}, a(b)_n} = \begin{bmatrix} j & t \\ -t & -j \end{bmatrix} \\ U_l = U_{a(b)_{n-1}, a(b)_n} = \begin{bmatrix} j & t \\ -t & -j \end{bmatrix}, \quad (7)$$

representing the transfer matrices for the rightward and leftward propagation along the chain “ a ” and “ b ”. U_\uparrow and U_\downarrow are given by

$$U_\uparrow = U_{a_n, b_n} = \begin{bmatrix} t_1 e^{i\theta_1} & t_2 e^{i\theta_2} \\ -t_2 e^{-i\theta_2} & -t_1 e^{-i\theta_1} \end{bmatrix} \\ U_\downarrow = U_{b_n, a_n} = \begin{bmatrix} t_1 e^{-i\theta_1} & t_2 e^{i\theta_2} \\ -t_2 e^{-i\theta_2} & -t_1 e^{i\theta_1} \end{bmatrix}, \quad (8)$$

representing the transfer matrices for the upward and downward propagation between the chain “ a ” and “ b ”.

The transfer matrix $U_{a(b)_m, a(b)_n}$ corresponds to the sub-matrix $\tilde{H}_{a(b)_m, a(b)_n}$ of dynamical matrix \tilde{H} under the basis $|\psi\rangle = [\dots, \gamma_{a_n}, \gamma_{b_n}, \dots]^\top$, as shown in Fig. 2(b). For the transition probability from site z_l to site z_0 after l hops, we can further introduce a notation $U_{z_0, z_l}^l = \sum_{z_1, z_2, \dots, z_{l-1}} U_{z_0, z_1} U_{z_1, z_2} \dots U_{z_{l-1}, z_l}$, where z_1, z_2, \dots, z_{l-1} are the sites experienced during these transitions, and the summation involves all possible paths. Similarly, U_{x_m, y_n}^l is the sub-matrix \tilde{H}_{x_m, y_n}^l of \tilde{H}^l .

The transfer matrix plays a key role in determining the confined area of the AB cage and the associated flat bands as shown below. The flat bands are usually formed by destructive interference [3, 4]. Here, the destructive interference of different transition paths can be effectively

captured by the transfer matrix as $U_{z_0, z_l}^l = 0$. Additionally, a single propagation path $U_{z_0, z_1} U_{z_1, z_2} \cdots U_{z_{l-1}, z_l} = 0$ can also confine the excitation through interference by the internal degrees of freedom within the transfer matrix.

The sufficient conditions for our system to form an AB cage is that the excitation at the n -th column cannot reach the $(n \pm 2)$ -th column. These conditions can be simplified as two limited single propagation path, as marked by the green and red lines in Fig. 2(c). To prevent transmission along the green propagation path, which lacks an equivalent path that interferes destructively with it, we require $U_l^2 = U_r^2 = 0$, yielding $j = t$ and $U_l = U_r$. For simplicity, we introduce the notation U_0 to represent both U_r and U_l . At the same time, since the green-marked path is prohibited and there is no equivalent path for destructive interference with the red-marked path, we further require the condition that

$$\begin{aligned} U_0 U_{\uparrow} U_0 &= U_0 U_{\downarrow} U_0 \\ &= 2j(t_1 \cos \theta_1 - t_2 \cos \theta_2) U_0 = 0, \end{aligned} \quad (9)$$

i.e., $t_1 \cos \theta_1 = t_2 \cos \theta_2$. It can be seen that the conditions for these two prohibited paths are precisely those for the flat band discussed in the previous section. This is because the flat band in momentum space arises from the constrained excitations in real space. In the Appendix B, we also demonstrate that these sufficient conditions are, in fact, necessary as well.

IV. DEGENERACY TYPE OF THE DFB

In this section, we clarify the degeneracy type of the DFBs using the transfer matrix. The underlying logic is that the degeneracy type of the eigenvalues is generally determined by the multiplicity of roots in the minimal polynomial, while the transfer matrix, as the sub-matrix of \tilde{H} , can be used to derive the minimal polynomial of \tilde{H} .

Given that each unit cell contains four degrees of freedom, the system can have at most four distinct flat bands. The order of the minimal polynomial of \tilde{H} thus cannot exceed 4 (the number of eigenvalues). Suppose the minimal polynomial of our system takes the form of

$$\tilde{H}^l + \sum_{n=0}^{l-1} c_n \tilde{H}^n, \quad (10)$$

with undetermined coefficients c_n and $l \leq 4$. The minimal polynomial is a factor of the annihilating polynomial of \tilde{H} , which has the form of $f(\tilde{H}) = d_4 \tilde{H}^4 + d_3 \tilde{H}^3 + d_2 \tilde{H}^2 + d_1 \tilde{H}^1 + d_0 I_{2N}$ with the order up to the numbers of eigenvalues and coefficients d_n . Using the transfer matrix, we can obtain different orders \tilde{H}^n , as detailed in the Appendix C. A combination of \tilde{H}^n up to the fourth power yields

$$(\tilde{H} - \lambda I)^2 (\tilde{H} + \lambda I)^2 = 0, \quad (11)$$

with $\lambda = \sqrt{t_1^2 - t_2^2}$. To determine the minimal polynomial from the above equation, we need to firstly identify its order. As we will demonstrate, the order of minimal polynomial is related to the dimension of invariant subspace formed during the evolution of state vectors, which is referred to as the local range of the excitation in this work.

Due to the inherent local nature within the AB cage, for an arbitrary excitation $|\psi\rangle_e$, the excitation transition either terminates at the end point of transition path or it returns to a linear combination of previously visited states after m times transition. Both of these two cases can be expressed as

$$\tilde{H}^m |\psi\rangle_e + \sum_{n=0}^{m-1} f_n \tilde{H}^n |\psi\rangle_e = 0. \quad (12)$$

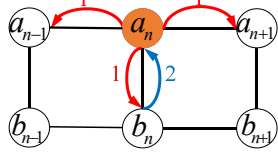
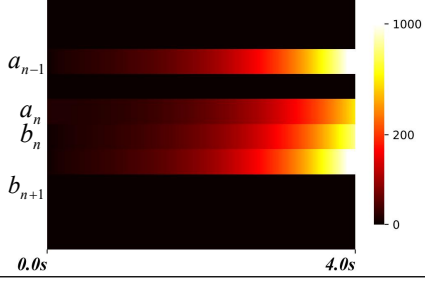
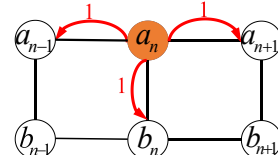
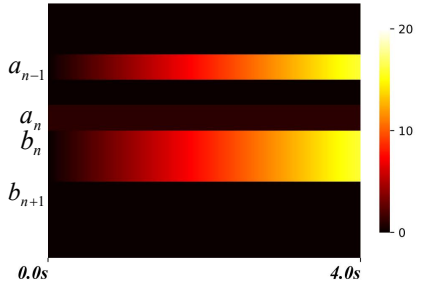
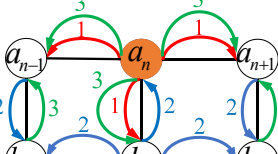
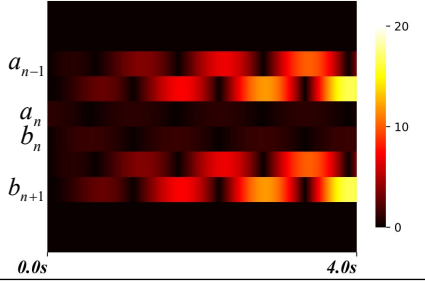
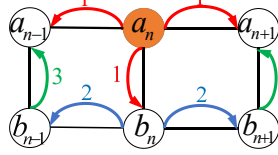
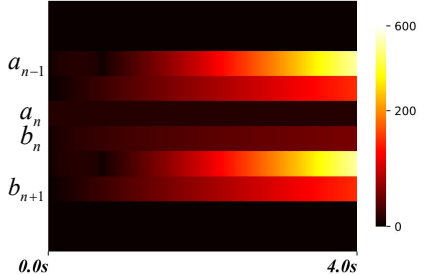
The coefficients f_n in the first case are zeros. The left side of the above equation is defined as the minimal polynomial of $|\psi\rangle_e$ in literature [58, 59]. Equation (12) shows that for an arbitrary excitation $|\psi\rangle_e$, the experienced linearly independent states $\{|\psi\rangle_e, \dots, \tilde{H}^{m-1} |\psi\rangle_e\}$ form a cyclic subspace with dimension m [57], implying that the evolution of $|\psi\rangle_e$ remains within this space. Thus, we can define this dimension m as the local range of the excitation $|\psi\rangle_e$. For excitations at different sites, the local ranges may take different values, and we denote the largest local range of excitations as the local range of AB cage. According to the Eq (10) of minimal polynomial, it is clear that the order l should be the upper bound of the local range. Furthermore, there always exists an excitation, whose minimal polynomial (Eq. (12)) is identical to the minimal polynomial of \tilde{H} [Eq. (10)] and the local range of AB cage is equal to l [59]. To prove this, we firstly utilize a mathematical corollary, which states that a matrix with minimal polynomial (10) can be similar to a block diagonal matrix containing the following matrix as diagonal block [57–59],

$$C = \begin{pmatrix} 0 & 0 & \cdots & 0 & -c_0 \\ 1 & 0 & \cdots & 0 & -c_1 \\ 0 & 1 & \cdots & 0 & -c_2 \\ \vdots & \vdots & & \vdots & \vdots \\ 0 & 0 & \cdots & 0 & -c_{l-2} \\ 0 & 0 & \cdots & 1 & -c_{l-1} \end{pmatrix}. \quad (13)$$

Applying the above matrix to a specified state $|e_k\rangle$ with l components, in which the subscript k indicates that only the k -th component is 1 with all other components being zero, we have

$$\begin{cases} |e_{k+1}\rangle = C |e_k\rangle, & \text{for } k < l; \\ C |e_l\rangle = -c_0 |e_1\rangle - c_1 |e_2\rangle - \cdots - c_{l-1} |e_l\rangle, & \text{for } l. \end{cases} \quad (14)$$

TABLE I. The intrinsic connection between the degeneracy type of DFBs, the minimum polynomial of \tilde{H} (first column), and the local range of AB cage (second column). The third column shows schematic diagram of the local range with the transition of initial excitation on a_n (orange color), where the arrows of different colors with numerical labels n indicate the n -th transition with the corresponding parameter conditions are shown above. The conditions $t_1 \cos \theta_1 = t_2 \cos \theta_2$, $j = t$ must always be held to form the AB cage. The local range is further verified by the numerical results of dynamical evolution under an initial state $\gamma^{a_n} = [1/\sqrt{2}, 1/\sqrt{2}]^\top$, as shown in the fourth column, where the color bar represents the intensity $|\gamma_{a_n(b_n)}|^2$ of wave function. The parameters for the numerical calculations are the same as those in Fig. 2(c).

Minimum polynomial	Local range	Excitation transition	Dynamical evolution
DP2: $(\tilde{H} - \lambda)(\tilde{H} + \lambda)$	2	$\theta_1 = n_1\pi, \theta_2 \neq n_2\pi$ $ t_1 \neq t_2 $ 	
1stEP2: \tilde{H}^2	2	$\theta_1 = n_1\pi, \theta_2 = n_2\pi$ $ t_1 = t_2 $ 	
2ndEP2: $(\tilde{H} - \lambda)^2(\tilde{H} + \lambda)^2$	4	$\theta_1 \neq n_1\pi, \theta_1 \pm \theta_2 \neq n_2\pi$ $ t_1 \neq t_2 $ 	
EP4: \tilde{H}^4	4	$\theta_1 \neq n_1\pi, \theta_1 \pm \theta_2 = n_2\pi$ $ t_1 = t_2 $ 	

The second equation can be simplified as

$$C^l |e_1\rangle + \sum_{n=0}^{l-1} c_n C^n |e_1\rangle = 0. \quad (15)$$

The collection of states $\{|e_1\rangle, \dots, |e_l\rangle\}$ forms a cyclic space with dimension l , which is the basis of the diagonal block (13), and the minimal polynomial of $|e_1\rangle$ is the same as the minimal polynomial (10) of \tilde{H} . Therefore,

the local range of excitation $|e_1\rangle$ can be l and the local range of the AB cage can take its upper bound, i.e., the order of minimal polynomial.

Having establishing the correspondence between the minimal polynomial in mathematic and the local range of AB cage in physics, now we can use them to clarify the degeneracy type of the DFBS, as shown in Table I. The excitations in different kinds of AB cage can generally transition differently with different local range, as visually presented in the third column in Table I. Since the leftward transition is symmetric about the rightward transition, we here only focus on the evolution of $[a_{n-1}, b_{n-1}, a_n, b_n]$ with the initial state $|\psi\rangle_e = [0, 0, \gamma_{a_n}, 0]$ (the third column in Table. I), where the arrow with number n indicates the n -th transition.

In the first two rows in Table I, the probability of excitation transition from a_n to $b_{n\pm 1}$ is zero. The transition probability $U_0U_\downarrow + U_\downarrow U_0 = 0$, leading to $\theta_1 = n_1\pi$, $t_1 \cos \theta_1 = t_2 \cos \theta_2$ with $n_1 \in \mathbb{Z}$. The corresponding state $H^n |\psi\rangle_e$ after n -th transition is denoted by $|\psi\rangle_n$ and

$$\begin{aligned} |\psi\rangle_1 &= [U_l \gamma_{a_n}, 0, 0, U_\downarrow \gamma_{a_n}]; \\ |\psi\rangle_2 &= [0, 0, U_\downarrow U_\uparrow \gamma_{a_n}, 0]. \end{aligned} \quad (16)$$

With $U_\uparrow U_\downarrow = (t_1^2 - t_2^2)I_2 = \lambda^2 I_2$ and $|t_1| \neq |t_2|$ in the first row in Table. I, the second state comes back to the position of initial state, $H^2 |\psi\rangle_e = \lambda^2 |\psi\rangle_e$. It will come to the same result when the excitation is at b_n . Thus for the single excitation at a_n , or b_n , or their linear combination, the largest local range is 2. The minimal polynomial with order 2 is

$$(\tilde{H} - \lambda I)(\tilde{H} + \lambda I), \quad (17)$$

which has two different single roots. Consider that each root is degenerate, therefore the system must have DP2s at eigenvalues $E = \pm\lambda$. The excitation transition is further verified by the numerical results of dynamic evolution in the fourth column in the Table. I, where the initial excitation $\gamma_{a_n} = [1/\sqrt{2}, 1/\sqrt{2}]^\top$ recovers to initial state after twice transitions. These numerical results also show exponential growth intensity at each sites, cause by positive imaginary eigenvalue $E = +\lambda$, since $\theta_1 = n_1\pi$, $t_1 = t_2 \cos \theta_2$, $|t_1| < |t_2|$ and λ is a imaginary number.

Different from the above case by only one condition $|t_1| = |t_2|$, the minimal polynomial $\tilde{H}^2 = 0$, implying that the emergence of EP2s at 0. It is the first kind of EP2s, denoted by 1stEP2s, corresponding to the second row in the Table. I. In this case, the transition is unidirectional. It stops after one transition at other sites instead of returning back the initial excitation position. The corresponding dynamical evolution shows that only the intensity at three sites $|\gamma_{a_{n\pm 1}}|^2$ and $|\gamma_{b_n}|^2$ near the excitation site grows linearly with the time due to the existence of EP2s, which aligns with the finding that the existence of EPns leads to n -order polynomial increase in the intensity of the n generalized eigenstates [45].

The other two rows in the Table. I show two degeneracy types, where the excitations at $a_n(b_n)$ can reach to the sites $b_{n\pm 1}(a_{n\pm 1})$ with $t_1 \cos \theta_1 = t_2 \cos \theta_2$, $\theta_1 \neq n_1\pi$. When $|t_1| \neq |t_2|$ (the third row in Table. I), with the initial excitation $|\psi\rangle_e$ at a_n , the excitation transition allows transition states including

$$\begin{aligned} |\psi\rangle_1 &= [U_l \gamma_{a_n}, 0, 0, U_\downarrow \gamma_{a_n}]; \\ |\psi\rangle_2 &= [0, (U_l U_\downarrow + U_\downarrow U_l) \gamma_{a_n}, \lambda^2 \gamma_{a_n}, 0]; \\ |\psi\rangle_3 &= [(2\lambda^2 U_l + U_\uparrow U_l U_\downarrow) \gamma_{a_n}, 0, 0, \lambda^2 U_\downarrow \gamma_{a_n}]. \end{aligned} \quad (18)$$

Along with the $|\psi\rangle_e$, there are four linearly independent states. The largest local range of such excitation is equal to the order of annihilating polynomial and thereby the minimal polynomial must be the annihilating polynomial.

Note that $|t_1| \neq |t_2|$ and $\lambda \neq 0$, the minimal polynomial has two different double roots and thus the system also has EP2s at $\pm\lambda$. Different from the previous 1stEP2s type with largest local range of 2, here the EP2s denoted by 2ndEP2s type possesses largest local range of 4. The heatmap of dynamical evolution also shows the intensity at sites a_n, b_n and $a_{n\pm 1}, b_{n\pm 1}$ oscillates with frequency λ , while the latter two sites are also accompanied by growth over time.

As for $|t_1| = |t_2|$, the minimal polynomial has a quadruple root and thus the system has EP4s at 0, which corresponds to the fourth row in the Table. I. All the transitions are unidirectional and excitation transition will end at the third transition state. The heatmap of dynamical evolution also shows that the intensity at the initial site keeps constant while intensity at $b_n, b_{n\pm 1}$, and $a_{n\pm 1}$ grows with time t due to the existence of EP4s.

In summary, we still use minimal polynomial to determine the degeneracy type of DFBS, while the minimal polynomial is obtained by the transfer matrix in two steps. The first step is to obtain the annihilating polynomial derived from the transfer matrix, whose factors include the minimal polynomial. The second step is to determine the local range, and hence the order of the minimal polynomial, by considering the transition of possible excitation through transfer matrix. Our results also suggest the AB cage with higher-order EPs generally has a larger local range.

V. THE CONSTRUCTION OF DFBS WITH $2N$ ORDER EXCEPTIONAL POINTS OF DEGENERACY (EP2NS)

In this section, we utilize the local range to construct DFBS with EP2Ns in coupled N bosonic Kitaev-Majorana chains, as illustrated in Fig. 3. Similar to previous notations, the transfer matrices propagating to the right or left along the chain m are denoted by U_r^m and

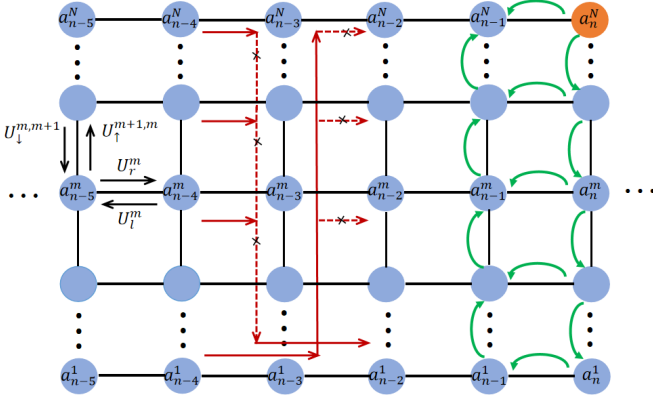


FIG. 3. The realization of AB cage with $2N$ -order EPs in N coupled bosonic Kitaev-Majorana chains. Left part: the transfer matrices along the corresponding directions are denoted by the black arrows. Middle part: the conditions for the formation of AB cage match those for the prohibited red propagation paths, which cause the excitation at the $(n-4)$ -th column to be localized between the $(n-5)$ -th column and $(n-3)$ -th column. Right part: the largest local range among possible excitations, illustrated by the allowed transitions (green lines).

U_l^m ,

$$U_r^m = U_l^m = t_m \begin{bmatrix} 1 & 1 \\ -1 & -1 \end{bmatrix} \propto U_0. \quad (19)$$

Here, the conjugated coupling and number non-conservation coupling are designed to have the same strength t_m , in order to meet the conditions for forming the flat band within a single chain. $U_{\downarrow(\uparrow)}^{m,m+1}$ represents the transfer matrices between the chain m and $m+1$,

$$U_{\uparrow}^{m+1,m} = \begin{bmatrix} t_1^{m,m+1} e^{i\theta_1^{m,m+1}} & t_2^{m,m+1} e^{i\theta_2^{m,m+1}} \\ -t_2^{m,m+1} e^{-i\theta_2^{m,m+1}} & -t_1^{m,m+1} e^{-i\theta_1^{m,m+1}} \end{bmatrix};$$

$$U_{\downarrow}^{m,m+1} = \begin{bmatrix} t_1^{m,m+1} e^{-i\theta_1^{m,m+1}} & t_2^{m,m+1} e^{i\theta_2^{m,m+1}} \\ -t_2^{m,m+1} e^{-i\theta_2^{m,m+1}} & -t_1^{m,m+1} e^{i\theta_1^{m,m+1}} \end{bmatrix}, \quad (20)$$

with conjugated coupling $t_1^{m,m+1} e^{i\theta_1^{m,m+1}}$ and number non-conservation coupling $t_2^{m,m+1} e^{i\theta_2^{m,m+1}}$. In the system with coupled two chains as discussed before, the additional prohibited propagation paths in Fig. 2 require the flat bands conditions include $U_0 U_{\uparrow} U_0 = U_0 U_{\downarrow} U_0 = 0$. Similarly, to maintain the flat bands in the system with N coupled chain, we require red propagation paths in Fig. 3 to be prohibited. The corresponding transfer matrices should satisfy

$$U_0 U_{\downarrow}^{m-x,m-x+1} \dots U_{\downarrow}^{m-1,m} U_0$$

$$= U_0 U_{\uparrow}^{m,m-1} \dots U_{\uparrow}^{m-x+1,m-x} U_0 = 0 \quad (21)$$

for arbitrary m and x with $x < m$.

To satisfy these conditions, a straightforward choice is to ensure

$$U_{\downarrow}^{m-1,m} U_0 = 0; \quad U_0 U_{\uparrow}^{m,m-1} = 0. \quad (22)$$

This requires $t_1^{m-1,m} = t_2^{m-1,m}$ and $\theta_1^{m-1,m} = -\theta_2^{m-1,m} \neq n_1 \pi$. These conditions precisely align with the requirement for combining two second-order EPs into a fourth-order EP in the double-chain system, resulting in arbitrary excitation at the $(n-4)$ -th column to be localized between adjacent the $(n-5)$ -th column and the $(n-3)$ -th column. Meanwhile, $t_1^{m-1,m} = t_2^{m-1,m}$ results in $U_{\downarrow}^{m-1,m} U_{\uparrow}^{m-1,m} = 0$. Along with $U_r^m U_l^m = 0$, each path in the system is unidirectional.

In order to determine the degeneracy type of this system, we need to find the annihilation polynomial of the system and determine the largest local range of the excitations in such AB cage. Now we consider an excitation $|\psi\rangle_e$ at site a_n^N (the orange point in Fig. 3) with transition paths shown in Fig. 3. Since the leftward transition is symmetric about the rightward transition, we here only consider the occupation of the transition states in the n -th and $(n-1)$ -th columns.

When the number of transitions m satisfies $1 \leq m \leq N-1$, the state after the m -th transition can be written as a superposition of different paths,

$$|\psi\rangle_m = \prod_{x=1}^m U_{\downarrow}^{N-x,N-x+1} |\psi\rangle_e + [\dots U_l^y \dots] |\psi\rangle_e. \quad (23)$$

The first term corresponds to the transitions that continuously occupy new site in the n -th column. The second term is a simplified notation for the transition to the $(n-1)$ -th column, which must involve a leftward propagation U_l^y with $y \geq 1$. As the number of transitions increases, the state in the n -th column will shift downwards one by one. Therefore, when $1 \leq m \leq N-1$, the states $|\psi\rangle_m$ are independent of each other, since they occupy different sites in the n -th column. The N -th transition results in multiplying U_l^1 in front of the first term. Therefore, for $N < m \leq 2N-1$, the state becomes

$$|\psi\rangle_m = \prod_{k=1}^{k=m-N} U_{\uparrow}^{k+1,k} U_l^1 \prod_{x=1}^{N-1} U_{\downarrow}^{N-x,N-x+1} |\psi\rangle_e$$

$$+ [\dots U_l^y \dots] |\psi\rangle_e, \quad (24)$$

with two terms corresponding to the evolution of two terms in Eq. (23). To determine independent states, we can still focus on the first term. It can be seen that the states in the $(n-1)$ -th column shift upwards one by one, thus contributing $N-1$ independent states. These states are also linear independent from previous states, due to no occupation on the n -th column. Therefore, after $(2N-1)$ times transitions, the set $\{|\psi\rangle_e, |\psi\rangle_1, \dots, |\psi\rangle_m\}$ consists of $2N$ independent states, and the local range of the excitation $|\psi\rangle_e$ can be $2N$. It is also worth noting that those transitions transfer the state from a_n^N to a_{n-1}^N , and the probability of further transitions is zero, i.e., $H^{2N} |\psi\rangle_e = 0$.

For other excitations at a_n^x , after $N + x - 1$ transitions, the state will be located at a_{n-1}^N and satisfy $\tilde{H}^{N+x} |\psi\rangle_e = 0$. Thus, for any linear combination of excitations on these lattice sites, the equation $\tilde{H}^{2N} |\psi\rangle_e = 0$ always holds. Therefore, the polynomial

$$\tilde{H}^{2N}, \quad (25)$$

is the annihilation polynomial of \tilde{H} . Since the system has an excitation with a local range of $2N$, the degree of the minimal polynomial should be greater than or equal to $2N$. Hence, the minimal polynomial of the system is given by equation (25), which has a degenerate root of multiplicity $2N$ at zero. Therefore, the system exhibits a flat band with an EP $2N$ s degeneracy.

VI. CONCLUSIONS

In conclusion, we propose a non-Hermitian AB cage in the bosonic BDG systems. Such AB cage is manifested as DFBS, where the degeneracy type can be flexibly controlled by the system parameters. The non-Hermitian nature in the BDG systems without introducing gain or loss and intrinsic symmetry facilitate the experimental realization. For example, the parametric amplification process in superconducting quantum circuits can be effectively implemented and regulated, which can serve as a candidate platform for the non-Hermitian AB cage. Theoretically, we build the correspondence among the degeneracy type of DFBS, the minimal polynomial, and the transfer matrix, and according to this, we design DFBS with arbitrarily high degeneracy. Our results provide theoretical guidance for designing the non-Hermitian AB cages and laying foundation on their dynamical properties. Currently, our work is limited to one-dimensional lattice systems, but our approach is expected to be extended to higher-dimensional systems, offering diverse platforms for studying strongly correlated physics.

This work is supported by the Natural Science Foundation of Hunan Province ((Grant No. 2024JJ6011) and Innovation Program for Quantum Science and Technology. (Grant No. 2021ZD0302300)

Appendix A: GAUGE INVARIANT NON-ABELIAN WILSON LOOP

Here, we explain that the chosen gauge can always ensure the phases only appear on the t_1 and t_2 , which is guaranteed by the gauge-invariant Wilson loop of the system. The particle and hole freedoms on a single site can be expressed by a two-component operator as $\gamma_{a_n(b_n)} = [\alpha_n(\beta_n), \alpha_n^\dagger(\beta_n^\dagger)]^\top$. According to the equation (6) in the main text, the effective Hamiltonian can

be written as

$$\tilde{H}_{eff} = \sum_{x_n, y_m} \gamma_{x_n}^\dagger U_{x_n, y_m} \gamma_{y_m}, \quad (A1)$$

with x_n, y_m traversing all sites. This can be viewed as a lattice Hamiltonian in the presence of a U(2) gauge field \mathbf{A} [55]. Here, the transfer matrix has the form of

$$U_{x_n, y_m} = J_{x_n, y_m} P \exp \left[i \int_{[y, m]}^{[x, n]} d\mathbf{x} \cdot \mathbf{A}(\mathbf{x}) \right], \quad (A2)$$

which is the link of the sites x_n and y_m multiplied by the uniform hopping strength J_{x_n, y_m} between the linked sites. Here, P is the path-order operator. For a given path that forms a loop, the gauge-invariant Wilson loop is defined as the trace of the product of link along the loop

$$W_{loop} = Tr(P \exp \left[i \oint d\mathbf{x} \cdot \mathbf{A}(\mathbf{x}) \right]). \quad (A3)$$

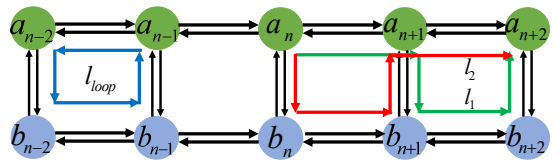


FIG. 4. The illustration of gauge-invariant Wilson loop and the sufficient and necessary conditions for the forming of AB cage. Left part: the blue path l_{loop} is a closed loop for excitation transition, and the trace of the link along such loop corresponds to a gauge-invariant Wilson loop. Right part: the excitations transition along the red path l_1 and green path l_2 to further sites when the transition along the chain is forbidden by the condition $j = t$. To form the AB cage, the excitation should only transition along such paths for finite periods.

Let's consider an excitation starting from site a_{n-2} and returning to its original position along the blue path l_{loop} in Fig. 4. The Wilson loop along the path is

$$W_{loop} = Tr(U_{loop}/J_{loop}). \quad (A4)$$

Here, $J_{loop} = J_{a_{n-2}, a_{n-1}} J_{a_{n-1}, b_{n-1}} J_{b_{n-1}, b_{n-2}} J_{b_{n-2}, a_{n-2}}$ is the hopping strength along the loop, and $U_{loop} = U_l U_\uparrow U_r U_\downarrow$ is the corresponding transfer matrix for this loop with the matrix form

$$U_{loop} = \begin{bmatrix} u_{1,1} & u_{1,2} \\ u_{2,1} & u_{2,2} \end{bmatrix}. \quad (A5)$$

The matrix elements of U_{loop} are calculated as follows,

$$\begin{aligned}
u_{1,1} &= [t_1^2(1 + e^{-i\Phi_1}) + t_1 t_2(e^{i\Gamma_1} + e^{-i\Gamma_2} + e^{i\Gamma_1} + e^{i\Gamma_2}) + t_2^2(1 + e^{-i\Phi_2})]tj, \\
u_{1,2} &= [t_1 t_2(2 + e^{-i\Phi_1} + e^{-i\Phi_2}) + t_2^2(e^{i\Gamma_1} + e^{i\Gamma_2}) + t_1^2(e^{i\Gamma_1} + e^{-i\Gamma_2})]tj e^{i(\theta_1 + \theta_2)}, \\
u_{2,1} &= [t_1^2(1 + e^{-i\Phi_1}) + t_1 t_2(e^{i\Gamma_1} + e^{-i\Gamma_2} + e^{i\Gamma_1} + e^{i\Gamma_2}) + t_2^2(1 + e^{-i\Phi_2})]tj e^{-i(\eta_a + \pi)}, \\
u_{2,2} &= [t_1 t_2(2 + e^{-i\Phi_1} + e^{-i\Phi_2}) + t_2^2(e^{i\Gamma_1} + e^{i\Gamma_2}) + t_1^2(e^{i\Gamma_1} + e^{-i\Gamma_2})]tj e^{-i\Gamma_1},
\end{aligned} \tag{A6}$$

where

$$\begin{aligned}
\Gamma_1 &= -\theta_1 - \theta_2 + \eta_a + \pi \\
\Gamma_2 &= -\theta_1 + \theta_2 - \eta_b + \pi \\
\Phi_1 &= 2\theta_1 + \eta_b - \eta_a \\
\Phi_2 &= 2\theta_2 - \eta_a - \eta_b
\end{aligned} \tag{A7}$$

The Wilson loop W_{loop} is invariant under a gauge transformation [55], which requires Φ_1 , Φ_2 , Γ_1 , and Γ_2 are gauge-invariant. Note that $\Gamma_1 + \Gamma_2 = -\Phi_1$ and $\Gamma_1 - \Gamma_2 = -\Phi_2$ and therefore θ_1 , θ_2 , η_a , and η_b only need to satisfy the third and fourth constraints in the above equations. When we take the gauge transformation $\alpha_n \rightarrow \alpha_n e^{i\varphi_a}$ and $\beta_n \rightarrow \beta_n e^{i\varphi_b}$,

$$\begin{aligned}
\theta_1 &\rightarrow \theta_1 + \varphi_b - \varphi_a, \\
\theta_2 &\rightarrow \theta_2 - \varphi_b - \varphi_a, \\
\eta_a &\rightarrow \eta_a - 2\varphi_a, \\
\eta_b &\rightarrow \eta_b - 2\varphi_b.
\end{aligned} \tag{A8}$$

It can be clearly seen that Φ_1 and Φ_2 don't change under the gauge transformation. Therefore, we can always perform a gauge transformation to apply all phases to the terms representing the coupling strengths between the two chains, such that $\eta_a = \eta_b = 0$, $\theta_1 = \Phi_1/2$, and $\theta_2 = \Phi_2/2$. Our subsequent calculations are based on this chosen gauge.

Appendix B: FLAT BAND CONDITIONS

The flat band conditions can be simplified as two limited propagation paths in the main text, as demonstrated below. The localization of excitation in single chain “ a ” or “ b ” requires $(U_r)^n = (U_l)^n = 0$ with integer n . For the case of $n = 1$, this corresponds to $U_r = U_l = 0$, implying that the sites are uncoupled, and therefore can be ignored. The dimension of $U_r = U_l$ constrains n , such that the case $(U_r)^2 = (U_l)^2 \neq 0$ but $(U_r)^3 = (U_l)^3 = 0$ cannot occur. Therefore, $n = 2$, which leads to $j = t$ and $U_r = U_l = U_0$. While for coupled two chains under conditions $U_r = U_l = U_0$ and $U_r^2 = U_l^2 = 0$, there are additional possible transition paths alternatively propagating two legs, such as $a_n \rightarrow b_{n+1} \rightarrow a_{n+2} \rightarrow b_{n+3} \rightarrow a_{n+4}$ periodically, as shown in Fig. 4. With $U_\uparrow U_\downarrow = (t_1^2 - t_2^2)I_2$,

the transfer matrix in one period from a_n to a_{n+2} is

$$\begin{aligned}
U_{a_{n+2}, a_n} &= (U_\uparrow U_0 + U_0 U_\uparrow)(U_\downarrow U_0 + U_0 U_\downarrow) \\
&= U_\uparrow U_0 U_\downarrow U_0 + U_0 U_\uparrow U_0 U_\downarrow,
\end{aligned} \tag{B1}$$

which is equal to the superposition of path l_1 (the green path in Fig. 4) with transfer matrix $U_1 = U_\uparrow U_0 U_\downarrow U_0$ and path l_2 (the red path in Fig. 4) with $U_2 = U_0 U_\uparrow U_0 U_\downarrow$.

For the formation of AB cage, the transition along the paths l_1 , l_2 can only sustain finite periods with $(U_{a_{n+2}, a_n})^m = 0$. Since the dimension of the U_{a_{n+2}, a_n} is 2, here m also can not be larger than 2. U_{a_{n+2}, a_n} has the form of

$$U_{a_{n+2}, a_n} = jt \begin{bmatrix} (t_1 \cos \theta_1 - t_2 \cos \theta_2)^2 & 0 \\ 0 & (t_1 \cos \theta_1 - t_2 \cos \theta_2)^2 \end{bmatrix}. \tag{B2}$$

It can be seen that $(U_{a_{n+2}, a_n})^2 = 0$ is equivalent to the equation (9) in the main text. Thus the conditions $t_1 \cos \theta_1 = t_2 \cos \theta_2$ and $j = t$ are both the necessary and sufficient conditions for the existence of an AB cage in our system.

Appendix C: ANNIHILATING POLYNOMIAL OF \tilde{H}

To obtain the annihilating polynomial, we first present the form of \tilde{H}^n with different orders. Without loss of generality, we only consider the case where the excitation is located at a_n , in the following discussion. The excitation at site a_n can propagate to b_n , a_{n+1} , and a_{n-1} as

$$\tilde{H}_{b_n, a_n} = U_\downarrow, \quad \tilde{H}_{a_{n+1}, a_n} = \tilde{H}_{a_{n-1}, a_n} = U_0 \tag{C1}$$

during the first transition. Note that all other sub-matrices of \tilde{H} not mentioned are zero matrices. During the second transition, the excitation can reach to sites b_{n+1} , b_{n-1} or come back to a_n . This results in the following nonzero sub-matrices

$$\tilde{H}_{a_n, a_n}^2 = U_\uparrow \tilde{H}_{b_n, a_n} = (t_1^2 - t_2^2)I_2; \tag{C2}$$

$$\begin{aligned}
\tilde{H}_{b_{n+1}, a_n}^2 &= \tilde{H}_{b_{n-1}, a_n}^2 = U_\downarrow \tilde{H}_{a_{n-1}, a_n} + U_0 \tilde{H}_{b_n, a_n} \\
&= U_\downarrow U_0 + U_0 U_\downarrow.
\end{aligned} \tag{C3}$$

After three transitions, the excitation returns to sites

b_n , a_{n+1} , and a_{n-1} , yielding

$$\begin{aligned}\tilde{H}_{b_n, a_n}^3 &= U_\downarrow \tilde{H}_{a_n, a_n}^2 + U_0 \tilde{H}_{b_{n-1}, a_n}^2 + U_0 \tilde{H}_{b_{n+1}, a_n}^2 \\ &= (t_1^2 - t_2^2) U_\downarrow;\end{aligned}\quad (\text{C4})$$

$$\begin{aligned}\tilde{H}_{a_{n+1}, a_n}^3 &= \tilde{H}_{a_{n-1}, a_n}^3 = U_0 \tilde{H}_{a_n, a_n}^2 + U_\uparrow \tilde{H}_{b_{n-1}, a_n}^2 \\ &= 2(t_1^2 - t_2^2) U_0 + U_\uparrow U_0 U_\downarrow.\end{aligned}\quad (\text{C5})$$

During the fourth transition, the excitation again reaches to sites b_{n+1} , b_{n-1} , and a_n , yielding

$$\begin{aligned}\tilde{H}_{a_n, a_n}^4 &= U_\uparrow \tilde{H}_{b_n, a_n}^3 + U_0 \tilde{H}_{a_{n+1}, a_n}^3 + U_0 \tilde{H}_{a_{n-1}, a_n}^3 \\ &= (t_1^2 - t_2^2)^2 I_2;\end{aligned}\quad (\text{C6})$$

$$\begin{aligned}\tilde{H}_{b_{n+1}, a_n}^4 &= \tilde{H}_{b_{n-1}, a_n}^4 = U_\downarrow \tilde{H}_{a_{n-1}, a_n}^3 + U_0 \tilde{H}_{b_n, a_n}^3 \\ &= 2(t_1^2 - t_2^2)(U_\downarrow U_0 + U_0 U_\downarrow).\end{aligned}\quad (\text{C7})$$

A combination of above \tilde{H}^n with different orders gives rise to the annihilating polynomial of \tilde{H} as

$$(\tilde{H} - \lambda I)^2 (\tilde{H} + \lambda I)^2 = 0, \quad (\text{C8})$$

which is the same as the result [Eq. (5)] previously obtained using γ matrix in momentum space.

* zengbowen@csust.edu.cn

† huyong@hust.edu.cn

- [1] V. Apaja, M. Hyrkäs, and M. Manninen, *Phys. Rev. A* **82**, 041402 (2010).
- [2] M. Hyrkäs, V. Apaja, and M. Manninen, *Phys. Rev. A* **87**, 023614 (2013).
- [3] S. Mukherjee, A. Spracklen, D. Choudhury, N. Goldman, P. Öhberg, E. Andersson, and R. R. Thomson, *Phys. Rev. Lett.* **114**, 245504 (2015).
- [4] R. A. Vicencio, C. Cantillano, L. Morales-Inostroza, B. Real, C. Mejía-Cortés, S. Weimann, A. Szameit, and M. I. Molina, *Phys. Rev. Lett.* **114**, 245503 (2015).
- [5] M. C. Rechtsman, J. M. Zeuner, A. Tünnermann, S. Nolte, M. Segev, and A. Szameit, *Nature Photonics* **7**, 153 (2013).
- [6] M. Biondi, E. P. L. van Nieuwenburg, G. Blatter, S. D. Huber, and S. Schmidt, *Phys. Rev. Lett.* **115**, 143601 (2015).
- [7] S. Deng, A. Simon, and J. Köhler, *Journal of Solid State Chemistry* **176**, 412 (2003), special issue on The Impact of Theoretical Methods on Solid-State Chemistry.
- [8] M. Imada and M. Kohno, *Phys. Rev. Lett.* **84**, 143 (2000).
- [9] H. Ramezani, *Phys. Rev. A* **96**, 011802 (2017).
- [10] L. Jin, *Phys. Rev. A* **99**, 033810 (2019).
- [11] Y. Zhang, S. Xia, X. Zhao, L. Qin, X. Feng, W. Qi, Y. Jiang, H. Lu, D. Song, L. Tang, *et al.*, *Photonics Research* **11**, 225 (2023).
- [12] T. Biesenthal, M. Kremer, M. Heinrich, and A. Szameit, *Phys. Rev. Lett.* **123**, 183601 (2019).
- [13] S. Weimann, L. Morales-Inostroza, B. Real, C. Cantillano, A. Szameit, and R. A. Vicencio, *Opt. Lett.* **41**, 2414 (2016).
- [14] S. Taie, H. Ozawa, T. Ichinose, T. Nishio, S. Nakajima, and Y. Takahashi, *Science Advances* **1**, e1500854 (2015), <https://www.science.org/doi/pdf/10.1126/sciadv.1500854>.
- [15] C. C. Abilio, P. Butaud, T. Fournier, B. Pannetier, J. Vidal, S. Tedesco, and B. Dalzotto, *Phys. Rev. Lett.* **83**, 5102 (1999).
- [16] Z.-H. Yang, Y.-P. Wang, Z.-Y. Xue, W.-L. Yang, Y. Hu, J.-H. Gao, and Y. Wu, *Phys. Rev. A* **93**, 062319 (2016).
- [17] J. Vidal, P. Butaud, B. Douçot, and R. Mosseri, *Phys. Rev. B* **64**, 155306 (2001).
- [18] J. Vidal, R. Mosseri, and B. Douçot, *Phys. Rev. Lett.* **81**, 5888 (1998).
- [19] S. Mukherjee, M. Di Liberto, P. Öhberg, R. R. Thomson, and N. Goldman, *Phys. Rev. Lett.* **121**, 075502 (2018).
- [20] H. Li, Z. Dong, S. Longhi, Q. Liang, D. Xie, and B. Yan, *Phys. Rev. Lett.* **129**, 220403 (2022).
- [21] S. Longhi, *Opt. Lett.* **39**, 5892 (2014).
- [22] J. Vidal, B. Douçot, R. Mosseri, and P. Butaud, *Phys. Rev. Lett.* **85**, 3906 (2000).
- [23] S. Li, Z.-Y. Xue, M. Gong, and Y. Hu, *Phys. Rev. A* **102**, 023524 (2020).
- [24] Z. G. Yuto Ashida and M. Ueda, *Advances in Physics* **69**, 249 (2020).
- [25] T. Yu, J. Zou, B. Zeng, J. Rao, and K. Xia, *Physics Reports* **1062**, 1 (2024).
- [26] W. Chen, Ş. Kaya Özdemir, G. Zhao, J. Wiersig, and L. Yang, *Nature* **548**, 192 (2017).
- [27] H. Hodaei, A. U. Hassan, S. Wittek, H. Garcia-Gracia, R. El-Ganainy, D. N. Christodoulides, and M. Khajavikhan, *Nature* **548**, 187 (2017).
- [28] M. P. Hokmabadi, A. Schumer, D. N. Christodoulides, and M. Khajavikhan, *Nature* **576**, 70 (2019).
- [29] R. Duggan, S. A. Mann, and A. Alù, *ACS Photonics* **9**, 1554 (2022), <https://doi.org/10.1021/acsphotonics.1c01535>.
- [30] T. Yu, J. Zou, B. Zeng, J. Rao, and K. Xia, *Physics Reports* **1062**, 1 (2024), non-Hermitian topological magnonics.
- [31] S. Sayyad and F. K. Kunst, *Phys. Rev. Res.* **4**, 023130 (2022).
- [32] I. Mandal and E. J. Bergholtz, *Phys. Rev. Lett.* **127**, 186601 (2021).
- [33] K. Wang, L. Xiao, H. Lin, W. Yi, E. J. Bergholtz, and P. Xue, *Science Advances* **9**, eadi0732 (2023), <https://www.science.org/doi/pdf/10.1126/sciadv.adi0732>.
- [34] P. Delplace, T. Yoshida, and Y. Hatsugai, *Phys. Rev. Lett.* **127**, 186602 (2021).
- [35] Y. Taguchi, M. Hirayama, and T. Miyake (2024).
- [36] B. Mera and J. Mitscherling, *Phys. Rev. B* **106**, 165133 (2022).
- [37] S. Becker, T. Humbert, and M. Zworski (2023).
- [38] W. Jiang, D. J. P. de Sousa, J.-P. Wang, and T. Low, *Phys. Rev. Lett.* **126**, 106601 (2021).
- [39] C. Le, Q. Zhang, F. Cui, X. Wu, and C.-K. Chiu, *Phys. Rev. Lett.* **132**, 246401 (2024).
- [40] S. M. Zhang, H. S. Xu, and L. Jin, *Phys. Rev. A* **108**, 023518 (2023).
- [41] S. Ke, D. Zhao, J. Fu, Q. Liao, B. Wang, and P. Lu, *IEEE Journal of Selected Topics in Quantum Electronics* **26**, 1 (2020).
- [42] S. M. Zhang and L. Jin, *Phys. Rev. Res.* **2**, 033127 (2020).
- [43] S. M. Zhang, T. Y. He, and L. Jin, *Chinese Physics Letters* **41**, 027201 (2024).

- [44] S. Lin, Y. Liang, J. Zhang, M. K. Chen, and D. P. Tsai, [Applied Physics Letters](#) **123**, 221103 (2023).
- [45] L. Ge, [Photonics Research](#) **6**, A10 (2018).
- [46] S. R. Garcia and R. A. Horn, *A second course in linear algebra* (Cambridge University Press, 2017).
- [47] B. A. Bernevig, *Topological insulators and topological superconductors* (Princeton university press, 2013).
- [48] A. Mostafazadeh, [TURKISH JOURNAL OF PHYSICS](#) (2020).
- [49] Y.-X. Wang and A. A. Clerk, [Phys. Rev. A](#) **99**, 063834 (2019).
- [50] H. Kondo, Y. Akagi, and H. Katsura, [Progress of Theoretical and Experimental Physics](#) **2020**, 12A104 (2020).
- [51] K. Yokomizo and S. Murakami, [Phys. Rev. B](#) **103**, 165123 (2021).
- [52] A. McDonald, T. Pereg-Barnea, and A. A. Clerk, [Phys. Rev. X](#) **8**, 041031 (2018).
- [53] L.-L. Wan and X.-Y. Lü, [Phys. Rev. Lett.](#) **130**, 203605 (2023).
- [54] J. K. Asbóth, L. Oroszlány, and A. Pályi, [Lecture notes in physics](#) **919** (2016).
- [55] Y. Makeenko, arXiv preprint arXiv:0906.4487 (2009).
- [56] A. Marsh, *Mathematics for Physics: An Illustrated Handbook* (World Scientific, 2017).
- [57] T. W. Hungerford, *Algebra*, Vol. 73 (Springer Science & Business Media, 2012).
- [58] N. Jacobson, *Basic algebra I* (Courier Corporation, 2012).
- [59] C. W. Curtis, *Linear algebra: an introductory approach* (Springer Science & Business Media, 2012).